2018 IEEE-RAS 18th International Conference on Humanoid Robots (Humanoids)
Beijing, China, November 6-9, 2018

Design of a single cam single actuator multiloop eyeball mechanism

Masood M Khan, *Member, IEEE* and Cheng Chen

***Abstract*—This paper reports design and implementation of a multiloop robotic eyeball mechanism that enables synchronously rotating two eyeballs using a single actuator. Our optimally designed eyeball mechanism can help in implementing light weight, agile and energy efficient robotic heads. To the best of our knowledge, no existing eyeball mechanism is able to synchronously rotate two eyeballs using a single actuator. This work demonstrates use of a multiloop mechanism for reducing the number of required actuators and hence reducing the overall power consumption. Our eyeball mechanism incorporates an optimally designed 4-PS (prismatic-spherical) plus 1-P (passive support) construct. This partially passive construct comprises of a double-dwell end-cam plus a 4-follower arrangement. The cam-follower arrangement also augments a control strategy for synchronously rotating eyeballs and irides. We also present a methodology for determining the position kinematics of this 4-degree of freedom robotic eyeball mechanism.**

***Index Terms*—Eyeball mechanism, multiloop construct, cam-follower system, robotic head design, sociable robots.**

I. Introduction

Socially intelligent robotic systems are expected to perform various intricate tasks such as greeting and serving customers in cafes [1]. The so called sociable robots can interact with people and are anticipated to replace human faces during socially engaging activities [1]. Such sociable robots will be required to communicate and respond to people in a human like manner [2]. The robotics community therefore need to device methods, tools and protocols for enabling social robots understand and express human behavior in a wide range of social situations[3] [4]. Glimpses of such capabilities are evident in some state-of-the-art sociable robots developed for education[5], entertainment [4], healthcare [6] and mental care sectors [7, 8].

The most intriguing features of sociable robots include an ability to exhibit human-like facial expressions while interacting with humans. During a human-human interaction, exhibition of affective states via facial expression is a natural phenomenon. Hence, expression of affective states will become an essential function in social robots as well. A few social robots have demonstrated ability of exhibiting facial expressions [9]. Experiencing and enjoying robots' expressions of affective states would make humans feel comfortable in social robots' company [10].

The human facial expression system is complicated and versatile as it exploits multiple groups of facial muscles for expressing affects [11]. Human eyes contribute to and augment exhibition of facial expressions [12]. Movements of eyelids and irides and their underlying mechanisms are important for display of facial expression [13]. The mechanism of human eyes is complex as it includes subsystems for rotating and moving eyeballs and eyelids; voluntarily and involuntarily. A robotic system can benefit by mimicking humans' ability to independently and separately move irides and eyelids. The irides' movements can be accomplished without engaging eyelids in a robotic eye system. This will need incorporating two mechanically independent and separate mechanisms in the eye system. This paper presents design and implementation of a simplified mechanism for achieving irides' movements.

As evident in the following paragraphs, simplification of an eyeball mechanism in this work was achieved by reducing the number of actuators and hence by reducing the degrees of freedom (DOF) of the mechanism. For reducing the number of actuators, a novel multiloop mechanism was also designed.

Multiloop linkages are suitable for systems that involve few prescribed positions of end effectors [14, 15]. The eyeball movement, in the presented design, would move the iris to a few identifiable positions during a social interaction. Hence, a multiloop mechanism, having more than one motion loops [16], could be employed for design simplification of the eyeball system.

Based on the mechanism design, multiloop system can require more than one degrees of freedom (DOF) for supporting the desired motion and scheme of robotic operations. However, some multiloop mechanisms can be designed to employ a smaller number of actuators than the number of loops in the system [17]. In particular, if a basic

This work was funded by the Faculty of Science and Engineering of Curtin University, Western Australia.

Cheng Chen is a graduate student in the Department of Mechanical Engineering, Curtin University, Western Australia (e-mail: cheng.chzn@graduate.curtin.edu.au).

Masood Mehmood Khan is with the Mechatronic Engineering group at the Faculty of Science and Engineering, Curtin University, Bentley, Western Australia (e-mail: masood.khan@curtin.edu.au).

motion loop can afford to possess several desired motion characteristics, less degrees of freedom (hence less number of actuators) are required for implementing a multiloop system [18].

The suitability of incorporating a multiloop mechanism in an spatial systems has been reported in several papers including [19] [17]. This works takes a step forward and combines the multiloop functionality with a support system to develop a light weight, agile and energy efficient eyeball mechanism. Hence, this work achieves two objectives; design of an optimally designed eyeball mechanism and minimize the number of required actuators.

This paper is organized in seven sections. Section II presents some of the relevant works. Section III reports the mechanism design. Section IV presents the iris position analysis approach. Sections V and VI respectively present the cam follower design and system implementation details. Section VII concludes this work.

II. Previous Works

Many innovative and novel robotic eyeball mechanisms have been developed in the recent past [2, 20-24]. Since this paper isn't focused on reviewing the existing eyeball mechanisms, only some of the relevant works are discussed here.

In [21], six pneumatic muscles were used to drive a 3-DOF humanoid robot eye. The employed eye movement patterns were ensured to be similar to those of a human eye. The robotic eye system exploited a parallel mechanism and the magnitude of actuation was enough to efficiently drive the system.

A parallel mechanism was considered plausible for incorporating the human eye like agility in a robotic eyeball mechanism [25]. It was demonstrated that using a spherical 3-DOF mechanism, a faster (than human eye) camera orienting ability could be achieved to cover a larger than human eye workspace. The agile eye, basically a parallel mechanism, used 3 rotatory actuators to perform.

In [26], an eyeball mechanism was incorporated in a robotic head. The head assembly was designed for moving cameras mounted to observe the environment. Each eye was basically a video camera fitted inside the eyeball. The cameras were rotated through a 3-DOF eyes mechanism. The neck mechanism had another 3-DOF for supporting the serial pitch, roll and yaw configurations. The three neck joints' movements and the eyes rotations were achieved using DC motors.

Apparently, the artificial muscle actuated mechanism [21] and the agile eye mechanism [25] would require a simple control strategy compared with the control strategy applied in [26]. However, these aforementioned eyeball mechanisms required multiple numbers of actuators to function. Generally speaking, the number of employed actuators in many of the existing eyeball systems were equal to their incorporated degrees of freedom. Hence these eyeball systems were fully actuated mechanisms. Also, these mechanisms could be termed as either planar rotatory or parallel manipulators.

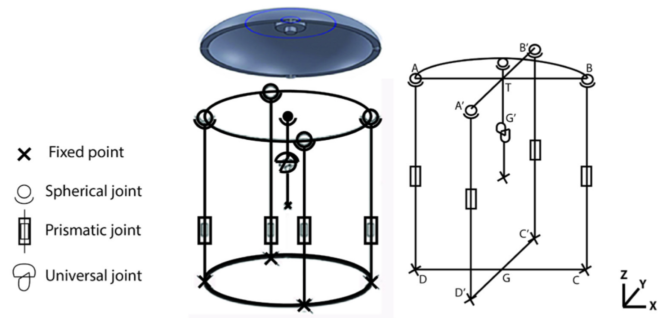

Fig. 1. Left - Legends. Middle - Geometric representation of hemispherical shape (above) and the 4-PS/1-PS mechanism (bottom) representing the eyeball system design. Right - Representation of the two pairs of congregate bars with prismatic joints fitted on them. Bars AD and BC form one congregate pair and bars A'D' and B'C' form the other congregate pair.

Building upon the existing eyeball designs and developments in multiloop manipulator analyses, we have designed a 4-DOF multiloop eyeball system that uses a single actuator to synchronously rotate the two eyeballs, has an optimal and light-weight mechanism and is robust.

III. Geometry of The Mechanism

Multiloop mechanisms are usually configured as planar manipulators [14, 16]. They can be incorporated in Stewart platform like constructs such that pairs of upper (adjacent) joint centres remain coincident while the multiple distinct joint centres form a planar convex quadrilateral and on the lower side (base platform), equal number (or more) of distinct joint centres form a planar convex polygon [16, 27]. These platforms are widely used in active systems such as flight simulators, surgical robots and 3D printers [28]. Several methods and analytical tools have been proposed to assess and synthesize mobility of such intrinsically spatial mechanisms and systems [14, 16, 17, 29].

The basic configuration of our robotic eyeball's multiloop mechanism is shown in Figure 1. It is a 4-PS (prismatic spherical)/1-P (passive support) system with the four active single-actuator supported PS links and an additional link at the center. The mechanism has five joint centers at the planar surface of the eyeball hemisphere. These joint centers form a closed planar convex quadrilateral on the circumferential periphery of the planar surface of the eyeball hemisphere. As shown in Figure 1, the lower links of the mechanism links are fixed at their respective centers. On the upper plane links are connected to the spherical joints and are mounted at their respective joint centers. The magnitude and direction of rotation of the moving plane (and hence of the eyeball and

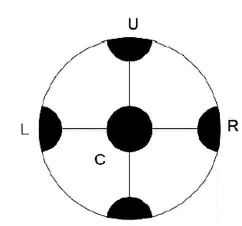

Fig. 2. Identified critical positions and teacks of the eyeball (and iris) movements.

irides) is determined by independent manipulation of each of the four prismatic joints. In this mechanism, the moving platform acts as a *de facto* end effector. However, because of the fixed DOF and as a consequence of actuation requirements, the end effector can only achieve a set of pre-defined arbitrary positions – suitable for a robotic eyeball movement. Hence, the underlying mechanism requires identification of a set of critical positions for the end effector (and irides) in order to express various affective states. Figure 2 shows the four assumed paths for achieving critical positions of the iris.

The position of the moving (upper) platform is initially parallel to the fixed (lower) plane and the iris is centered at position *C* (Figure 2). The four linkages are connected to the eyeball at points *L, R, U* and *D* in Figure 2. When any of the prismatic joints is pulled forward, a congruent joint (and bar) is pushed backward toward a pre-defined critical position. The planar surface of the eyeball moves along the solid lines (Figure 2) to eventually reach any of the desired positions.

A realistic robotic eyeball system would require a combination of two independent, synchronized (in terms of path and rotation) and simultaneously responding 4-bar linkages; hence a multiloop operation. The basic geometry for achieving such a functionality in our multiloop mechanism is shown in Figure 1. The midpoints of CD and $C'D'$ are fixed at the origin *G*. In order to move the iris, one of the links AD, $A'D'$, BC or $B'C'$ must move along the z-axes which is the axis of translation of every prismatic joint in the mechanism. A forward push applied to any of the points D, D', C and C' will result in either up-down or left-right movement about the point T. Since it is a simple mechanism, the actuator is not required to separately control movements of individual links AD, $A'D'$, BC and $B'C'$. The force pushing a particular link

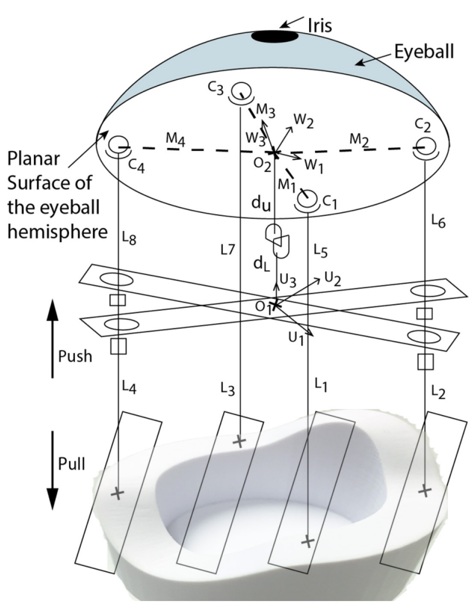

Fig. 3. The 4-PS/1-PS arrangement showing all the links, joints, planes and a cam that make up the multiloop mechanism. The two coordinate systems O_1 and O_2 provide bases for kinematic analysis of this mechanism. The push-pull effect of cam rotation is obvious.

backward would act only on a single point from among D, D', C and C' at a time. For example, when D' is pushed forward, the congruent bar $B'C'$ passively moves backward while links AD and BC remain stationary and the link $G'T$ experiences a corresponding rotation. The length of the link $G'T$ can also be used to restrict the movement of links AD and BC and hence rotation of the iris. When D' is being pushed, as obvious in Figures 1 and 2, the hemispherical eyeball will rotate about the x-axis. The magnitude of rotation is determined by the magnitude of displacement caused by pushing the point D' forward.

Kinematic design like ours could result in a hyperstatic kinematic model [30]. Hyperstatic models can produce over-constrained mechanisms [31, 32]. Our design approach relies on superposition of two kinematic modules and ensures that the combination of two models produces adequate angles between the platforms, links and joints; as in a typical Stewart platform [15, 33, 34]. A combination of the two simple kinematic modules can make it possible to develop a better yet less complicated mechanism [33,34].

IV. Direct Position Analysis Approach

Approaches used for position analyses of similar mechanisms have been discussed in several paper including [29, 30, 33, 34]. The multiloop eyeball mechanism, shown in Figure 3, would assume an equal length of links L_1 to L_4 and links L_5 to L_8 while the iris is posed in neutral position. The lengths of links d_L and d_u need not be the same as the length of link d_u could be varied for restricting the rotation of the iris. One end of links L_1 to L_4, shown in Figure 3, is fixed at the base and the other end is connected to a prismatic joint. Lower ends of links L_5 to L_8 are connected to prismatic joints and the other ends are connected to spherical joints. The spherical joints are connected to the lower planar surface of the eyeball hemisphere. Positions of links L_1 to L_4 can be analyzed in relation to the origin $O_1(U_1, U_2, U_3)$ having Cartesian coordinates. Movements of links L_1 to L_4 are constrained along axes U_1, U_2 to 1-DOF, so they move only along the vertical (U_3) axis of O_1. An arbitrary frame $O_2(W_1, W_2, W_3)$ is assigned to the center of the planar surface of the hemispheric eyeball such that the axes W_1 and W_2 form two coordinates of the planar surface.

The four spherical joints on the planar surface of the eyeball hemisphere are functionally divided into two groups; each group contains a pair of two congruent joints. The set of two congruent spherical joints would rotate in unison such that the magnitude and directions of rotation of the two congruent joints always remain the same. The centres of rotation of joints C_i (i = 1,...,4) will be centered along the lengths of links L_5-L_8. Frames O_1, and O_2 provide the geometric relationships required for the kinematic analysis of links and joints. The equations required for determining an arbitrary position of the iris can be derived by the geometric relationships between frames O_1, and O_2. For example, when L_4 is pushed forward, constrained by the degrees of freedom of multiple joints, the planar surface of eyeball hemisphere would have a single degree of freedom and will move about W_1 axis such that its position will be expressed by the following matrix as shown in (Figure 3)

$$\begin{bmatrix} & R_{O_1}^{O_2} & & d_{u}{}_{O_1}^{O_2} \\ 0 & 0 & 0 & 1 \end{bmatrix}.$$

Note that the link d_L remains passive whereas link d_u is active although it is not actuated. Thus d_u behaves like a passive link. As shown in the following sections, the direct kinematic singularities of this mechanism are controlled by constraining movements of links.

An arbitrary orientation of the moving planar surface can be represented through a unit vector of rotation $\overline{\boldsymbol{O}}$ and a set of three unit vectors $\hat{\jmath}, \hat{k}$ and $\hat{l}$ associated with the vector $\overline{\boldsymbol{O}}$. As shown in Figure 3, vectors $\hat{\jmath}, \hat{k}$ and $\hat{l}$ are geometrically linked to O_2 and joints C_i (i=1-3) as:

$$\hat{\jmath} = [j_1\ j_2\ j_3]^T = \frac{\overrightarrow{O_2C_1}}{|\overrightarrow{O_2C_1}|}; \tag{1}$$

$$\hat{k} = [k_1\ k_2\ k_3]^T = \frac{\overrightarrow{O_2C_2}}{|\overrightarrow{O_2C_2}|} \text{ and;} \tag{2}$$

$$\hat{l} = [l_1\ l_2\ l_3]^T = \frac{\overrightarrow{O_2C_3}}{|\overrightarrow{O_2C_3}|}. \tag{3}$$

Considering the algebraic characteristics of the shown system, the unit vector $\overline{\boldsymbol{O}}$ can define any orientation of the moving plane in terms of the two unit vectors as:

$$\overline{\boldsymbol{o}} = \begin{bmatrix} o_1 \\ o_2 \\ o_3 \end{bmatrix} = \vec{R} = \begin{bmatrix} j_1 \\ j_2 \\ j_3 \end{bmatrix} \times \begin{bmatrix} k_1 \\ k_2 \\ k_3 \end{bmatrix}. \tag{4}$$

Using a simple vector resolution method, the rotation vector $\overline{\boldsymbol{O}}$ can be calculated as:

$$\overline{\boldsymbol{o}} = [o_1\ o_2\ o_3]^T = \frac{\vec{R}}{|\vec{R}|}. \tag{5}$$

Being the cross product of the two unit vectors, $\overline{\boldsymbol{O}}$ would remain oriented along either W_1 axis or W_3 axis, depending on the link being pushed forward. In order to estimate an arbitrary orientation of the moving plane of the eyeball hemisphere (and irides), the three components of $\hat{\jmath}$ and the three components of $\hat{k}$ need to be considered. Hence, determining an arbitrary position would require these six parameters and an estimate of d_u; hence seven parameters.

Considering D_i a (unit) direction vector of vector $\overrightarrow{L_iC_i}$ and p_i be a position vector of L_i in the reference frame O_1 such that $p_i = O_1L_i = [p_{i1}\ p_{i2}\ p_{i3}]^T; (i = 1,..4)$. Note that vectors $M_i; (i = 1,..4)$ can be given as: $M_1 = m_1\hat{\jmath}$; $M_2 = m_2\hat{\jmath}$; $M_3 = m_3\hat{\jmath}$ such that $m_i = O_2C_i$; $(i = 1,..3)$. The vector M_4 can be obtained as

Fig. 4. The purpose-built concave and convex contours of the designed end-cam.

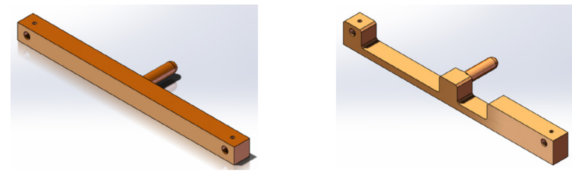

Fig. 5. The two geometric configurations of the pointed followers used in the cam-follower system.

$M_4 = S_1M_1 + S_2M_2 + S_3M_3$ where S_1, S_2 and S_3 are coefficients of M_1, M_2 and M_3 respectively. The following equations can represent the mechanism:

$$p_1 + D_1 = d + M_1; \tag{6}$$

$$p_2 + D_2 = d + M_2; \tag{7}$$

$$p_3 + D_3 = d + M_3 \text{ and;} \tag{8}$$

$$p_4 + D_4 = d + M_4. \tag{9}$$

Note that $d = d_L + d_U$ in equations 6-9.

For the basic characteristics of vectots the three unit vectors $\hat{\jmath}, \hat{k}$ and $\hat{l}$ would result in the following representations;

$$\textstyle\sum_{i=1}^{3} \hat{\jmath_i}^2 = 1 \tag{10}$$

$$\textstyle\sum_{i=1}^{3} \hat{k_i}^2 = 1 \tag{11}$$

$$\textstyle\sum_{i=1}^{3} \hat{l_i}^2 = 1 \tag{12}$$

$$\textstyle\sum_{i=1}^{3} \hat{\jmath}_i \cdot \hat{k}_i = \delta_1 \tag{13}$$

$$\textstyle\sum_{i=1}^{3} \hat{k}_i \cdot \hat{l}_i = \delta_2 \tag{14}$$

$$\textstyle\sum_{i=1}^{3} \hat{\imath}_i \cdot \hat{l}_i = \delta_3. \tag{15}$$

In the above equations, δ represents the angle given as $\delta_i = cos\psi_i$ and ψ_i represents an angle between any two corresponding vectors.

The following features of this construct minimize the level of system complexity. First, $\overrightarrow{O_2C_1}$ is collinear with $\overrightarrow{O_2C_3}$ and $\overrightarrow{O_2C_2}$ is collinear with $\overrightarrow{O_2C_4}$. Second, the end-cam shown in Figure 4, uniformly distributes the applied force around the fixed end at the base O_1. The resulting system will therefore be a twelfth-order polynomial, giving at least twelve position of the irides along the lines shown in Figure 2 [6, 15]. This twelfth-order polynomial can be expressed as:

$$\textstyle\sum_{i=1}^{12} Y_i d_i = 0. \tag{16}$$

The parameter Y_i in equation (16) depends on the parameters of the mechanism. Notice that the lower plane of the mechanism in Figure 3 is activated through a cam follower arrangement.

Please note that for the space limitations, an abridged account of the kinematic analysis is being presented in this

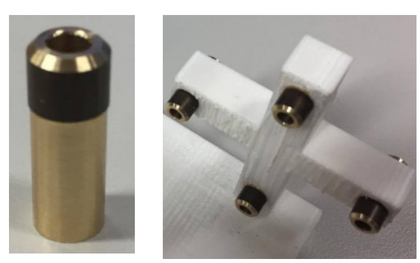

(a) (b)

Fig. 6. (a). A linear bush to keep the links L_1 to L_4 aligned and (b) A set of four linear bearings mounted inside the support structure that keeps the links straight and attached to the eyeball.

paper. The following section explains how the system is actuated for achieving a desired orientation of the irides.

V. The Cam-Follower System Design

The cam-follower system was designed and incorporated to ensure that the output displacement remains a function of the input displacement in a mechanism. In addition to converting the rotatory displacement input into a desired translational output motion, the cam-follower system in this work helps in achieving the desired actuation of the multiloop system. The purpose-built cam follower configuration has an end-cam, shown in Figure 4. A set of four pointed followers were mounted on the lower planar bars (of the base) using two different geometries for avoiding any friction and collision between the system components (as in Figure 5). The cam-follower system feeds in a single rotary displacement function to the two independent eyeballs (closed loop mechanisms) and makes them undergo the same magnitude of displacement, in the same direction, in a synchronized manner. The movements of the two eyeball mechanisms are constrained such that the designed cam-follower system provides a reliable and conventional power transmission mechanism. Using its two main parts; the end-cam and pointed followers, the cam- follower system offers the required motion loops. Such an end-cam and pointed followers combination is suitable for low velocity, low force and horizontal displacement systems [14].

Some constraining fittings and springs (shown in Figure 6) were used to keep the pointed followers in contact with the end-cam and control the system singularities. Hence, the cam follower configuration forces the links to move along the working surface. The convex portion of the cam pushes the follower forward. This forward push would cause a prescribed rotation of the eyeball planar surface and hence of the eyeball hemisphere. Whenever a particular link is pushed forward, its congruent link passively moves in opposite direction. The position of the passively moving link is constrained by the concave geometry of the cam. In order to support a smooth translation of the two active links, the degrees of freedom are effectively constrained by adding supporting structures; shown in Figure 6. This structural arrangement enables each of the four cam followers to control the eyeball hemisphere's rotation. Moreover, the followers are connected with the bar segments placed at the base of the multiloop mechanism. As obvious in Figure 6, the movement of any of these base bars is aligned by the linear bearings. In order for the links to work as conjugates, compression springs are placed between the hemispherical eyeballs and linear bearings. Compression springs retain followers' positions and directions with respect to the working surface of the cam. These springs pose a great majority of the work load to the cam. The load, during an eyeball movement cycle varies within a small range according as the system requirements. Based on the dynamics analysis, the selected springs having nominal dimension of $3.932 \times 25.4 \times 0.279$ mm were used. The cam is actuated in clockwise and anti-clockwise directions by a 5V stepper motor. A simulation based speed of 30 revolutions per minute (RPM) was set as the default rotating speed. However, the maximum and minimum rotating speeds can be increased or decreased depending on the affect expression requirements and the control strategy. This design allows the control strategy to easily modify the operating speed of the cam. Figure 7 shows SVA curves of the cam-follower program. Since a stepper motor is used in this mechanism, the control scheme is simple and easy to modify.

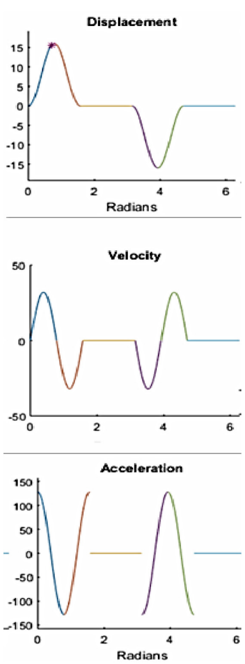

Fig. 7. SVA curve of the cam. (Top) The displacement curve. (Middle) The velocity curve. (Bottom) The Acceleration curve.

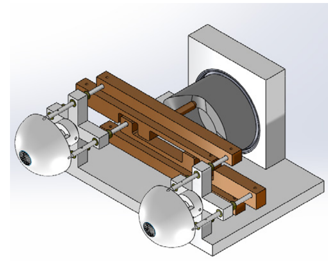

Fig. 8. A computer generated 3-D image of the multiloop eyeball system.

VI. Implementation of The Mechanism

The novelty and prominent aspects of this work emanate from the fact that it exploits the flexibility of a multiloop mechanisms. This design replaces multiple actuators needed to rotate the eyeballs, with a single actuator and a cam follower arrangement. Achieving actuation through such a combination of multiple sub-systems might be useful for many other applications. As obvious in Figure 8, the cam follower system requires only one rotary actuator to let the robotic eyeball mechanism function.

The mechanism and overall design of the eyeball system enable simultaneous, synchronized and single-motor actuated

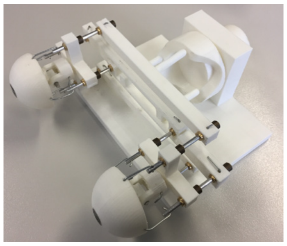

Fig. 9. The 3-D printed and assembled eyeball system.

movements of the two eyeballs. The base on which the four links rest was designed and optimized to ensure that each link can be pushed forward by a prescribed amount for achieving the desired arbitrary positions of the two eyeballs. The four followers sit at the four corners (90 ° apart from each other) on the base. Though the base can be implemented in several other ways, this optimal design has the following advantages.

First, the weight and dimensions of each individual bar can be reduced to develop a light-weight base, compared with a single solid base. Second, a smaller and less energy intensive actuator can be employed to push forward a desired link such that its associated link can be pushed back passively. Third, based on the first two factors, the overall power requirement of the system is much less compared with many of the existing eyeball mechanisms. Lastly, the presented mechanism is simpler and easy to incorporate in a robotic head.

In this implementation, ranges of pitch and yaw movements of eyeballs were kept around $\pm 30°$. In order to approach an object at an oblique angle, a combined motion of head, neck and eyeball mechanisms will be required. As obvious in Figures 8 and 9, the eyeball mechanism, being able to move the irides in up, down, left and right positions, can be synchronized with the head and neck movements for exhibiting various facial expressions.

The current system, shown in Figure 9, is a 3-D printed scaled up version of the actual system. The current 3-D printed version of the system can be adequately scaled for adaption and inclusion in a robotic head. The eyeball system meets the requirements of efficient actuation and simplified geometry and structure. It needs a simple control strategy to perform in synchrony with a robotic head. The complete eyeball system comprises of only twenty-five parts; much less than the number of components used in many of the exiting eyeball systems. The auxiliary components needed for the system include a deep groove ball bearing with 40 mm inner diameter and 68 mm outer diameter. A set of eight linear bearing with 3 mm inner diameter and 7 mm outer diameter was also used in the system. Each link moves through a linear bearing. The connecting shafts are made of stainless steel and have 3 mm diameters. Notice that each shaft has two holes on it for connecting the eyeballs, shafts and the follower blocks.

Table I presents magnitudes of movements and rotations incorporated in the system. A simple control algorithm, stored on a microcontroller, controls the stepper motor and cam-follower motion for moving the links and the rotating eyeball loops. A high gain amplifier was used in the circuit to amplify the output voltage. The system was tested at various speeds

TABLE I
MOTION PARAMETERS OF HUMAN EYEBALL AND THE PROPOSED EYEBALL

Parameter	Human eyeball	*This eyeball mechanism
Eyeball diameter [35]	24 mm	25 mm
Iris diameter[36]	12 mm	12 mm
Average inter-pupillary distance in mm [37]	*Male:64.7 Female: 62.3*	64 mm
*Pitch angle[38]***	*80 °*	78 °
Moving range of human eyes; based on [35]	*Up: 35° Down: 35° Left: 35° Right: 35°*	*Up: 35° Down: 35° Left: 35° Right: 35°*
*Yaw angle [38]***	90 °	90 °

*The reported eyeball model is a 2X scaled up model.
**estimated measurements are based on [38].

but a default rotating speed of 30 RPM was found to be suitable for displaying common facial expressions.

Weight of each major component and the overall weight of the eyeball mechanism are presented in Table II.

VII. CONCLUSION

This work demonstrates how the intrinsic mobility of a spatial multiloop system can be exploited to achieve arbitrary positions for synchronously rotating two robotic eyeball mechanisms. The work also demonstrates application of a purpose-built end-cam and follower configuration for synchronized control of two similar eyeball mechanisms. This eyeball system design and implementation can be helpful in producing artificial eyeball systems for humanoid robots. Through a novel and suitable configuration of multiloop mechanisms and a cam-follower arrangement, we were able to simplify the eyeball design and reduce its actuation requirements. The eyeball system presented in this work uses a single actuator to control both eyeball mechanisms. To the best of authors' knowledge, no other eyeball mechanism has so far been able to synchronously rotate two eyeball systems

TABLE II
WEIGHTS OF MAJOR EYEBALL SYSTEM COMPONENTS*

Component	Weight in grams
Linear bush	8 x 3 g
End-cam	1 x 94 g
Eyeball	2 x 8 g
Follower I (bars)	2 x 7 g
Follower I (bars)	2 x 8 g
***Overall system with mount and base*	290 g

*The reported components' weights are based on a 2X scaled up model.
** Actuator and electronic modules' weights not included.

using a single incremental electric motor.

The multiloop mechanism, basically a 4-DOF, 4-PS/1-P system, presented in this work was able to control the system singularities. The kinematic analysis is evident that the design is free of a hyperstatic mechanism's characteristics as the system is not an over-constrained structure. The system is able to effectively yet parsimoniously operate an eyeball system for longer durations. The presented design is expected to contribute to solutions of the common structural complexities and control related problems of spatial parallel mechanisms.

REFERENCES

[1] M.-T. Chu, R. Khosla, S. M. S. Khaksar, and K. Nguyen, "Service innovation through social robot engagement to improve dementia care quality," *Assistive Technology,* vol. 29, pp. 8-18, 2017.

[2] A. Takanishi, S. Ishimoto, and T. Matsuno, "Development of an anthropomorphic head-eye system for robot and human communication," in *Robot and Human Communication, 1995. RO-MAN'95 TOKYO, Proceedings., 4th IEEE International Workshop on*, 1995, pp. 77-82.

[3] N. Mavridis, "A review of verbal and non-verbal human–robot interactive communication," *Robotics and Autonomous Systems,* vol. 63, pp. 22-35, 2015.

[4] T. Kanda and H. Ishiguro, *Human-robot interaction in social robotics*: CRC Press, 2017.

[5] M. Zakipour, A. Meghdari, and M. Alemi, "RASA: a low-cost upper-torso social robot acting as a sign language teaching assistant," in *International Conference on Social Robotics*, 2016, pp. 630-639.

[6] S. Zarkandi, M. Daniali, and R. Hamid, "Direct kinematic analysis of a family of 4-DOF parallel manipulators with a passive constraining leg," *Transactions of the Canadian Society for Mechanical Engineering,* vol. 35, pp. 438-459, 2011.

[7] A. G. Pour, A. Taheri, M. Alemi, and A. Meghdari, "Human–Robot Facial Expression Reciprocal Interaction Platform: Case Studies on Children with Autism," *International Journal of Social Robotics,* pp. 1-20, 2018.

[8] R. Riener, T. Nef, and G. Colombo, "Robot-aided neurorehabilitation of the upper extremities," *Medical and biological engineering and computing,* vol. 43, pp. 2-10, 2005.

[9] D. Benson, M. M. Khan, T. Tan, and T. Hargreaves, "Modeling and verification of facial expression display mechanism for developing a sociable robot face," in *Advanced Robotics and Mechatronics (ICARM), International Conference on*, 2016, pp. 76-81.

[10] C. Breazeal, "Social robots: from research to commercialization," in *Proceedings of the 2017 ACM/IEEE International Conference on Human-Robot Interaction*, 2017, pp. 1-1.

[11] M. M. Khan, R. D. Ward, and M. Ingleby, "Toward Use of Facial Thermal Features in Dynamic Assessment of Affect and Arousal Level," *IEEE Transactions on Affective Computing,* vol. 8, pp. 412-425, 2017.

[12] H. Miwa, T. Okuchi, K. Itoh, H. Takanobu, and A. Takanishi, "A new mental model for humanoid robots for human friendly communication introduction of learning system, mood vector and second order equations of emotion," in *Robotics and Automation, 2003. Proceedings. ICRA'03. IEEE International Conference on*, 2003, pp. 3588-3593.

[13] Y. Zhang, J. Liu, K. Qi, and Z. Liu, "Modeling, design and analysis of a biomimetic eyeball-like robot with accommodation mechanism," in *Robotics and Biomimetics (ROBIO), 2013 IEEE International Conference on*, 2013, pp. 861-866.

[14] H. D. Eckhardt, *Kinematic design of machines and mechanisms*: McGraw-Hill New York, 1998.

[15] N.-X. Chen and S.-M. Song, "Direct position analysis of the 4–6 Stewart platforms," *Journal of Mechanical Design,* vol. 116, pp. 61-66, 1994.

[16] C. Galletti and E. Giannotti, "Multiloop kinematotropic mechanisms," in *ASME 2002 International Design Engineering Technical Conferences and Computers and Information in Engineering Conference*, 2002, pp. 455-460.

[17] H. Huang, Z. Deng, X. Qi, and B. Li, "Virtual chain approach for mobility analysis of multiloop deployable mechanisms," *Journal of Mechanical Design,* vol. 135, p. 111002, 2013.

[18] F. Freudenstein and E. Maki, "The creation of mechanisms according to kinematic structure and function," *Environment and Planning B: Planning and Design,* vol. 6, pp. 375-391, 1979.

[19] D. Gan, J. Dias, and L. Seneviratne, "Unified kinematics and optimal design of a 3rRPS metamorphic parallel mechanism with a reconfigurable revolute joint," *Mechanism and Machine Theory,* vol. 96, pp. 239-254, 2016.

[20] R. Beira, M. Lopes, M. Praça, J. Santos-Victor, A. Bernardino, G. Metta*, et al.*, "Design of the robot-cub (icub) head," in *Robotics and Automation, 2006. ICRA 2006. Proceedings 2006 IEEE International Conference on*, 2006, pp. 94-100.

[21] X.-y. Wang, Y. Zhang, X.-j. Fu, and G.-s. Xiang, "Design and kinematic analysis of a novel humanoid robot eye using pneumatic artificial muscles," *Journal of Bionic Engineering,* vol. 5, pp. 264-270, 2008.

[22] S.-C. Shen and J.-C. Huang, "Design and fabrication of a high-power eyeball-like microactuator using a symmetric piezoelectric pusher element," *Journal of microelectromechanical systems,* vol. 19, pp. 1470-1476, 2010.

[23] A. Parmiggiani, M. Maggiali, L. Natale, F. Nori, A. Schmitz, N. Tsagarakis*, et al.*, "The design of the iCub humanoid robot," *International journal of humanoid robotics,* vol. 9, p. 1250027, 2012.

[24] C. M. Gosselin and J. F. Hamel, "The agile eye: a high-performance three-degree-of-freedom camera-orienting device," in *Proceedings of the 1994 IEEE International Conference on Robotics and Automation*, 1994, pp. 781-786 vol.1.

[25] C. M. Gosselin and J.-F. Hamel, "The agile eye: a high-performance three-degree-of-freedom camera-orienting device," in *Robotics and Automation, 1994. Proceedings., 1994 IEEE International Conference on*, 1994, pp. 781-786.

[26] N. G. Tsagarakis, G. Metta, G. Sandini, D. Vernon, R. Beira, F. Becchi*, et al.*, "iCub: the design and realization of an open humanoid platform for cognitive and neuroscience research," *Advanced Robotics,* vol. 21, pp. 1151-1175, 2007.

[27] A. Kecskemethy, T. Krupp, and M. Hiller, "Symbolic processing of multiloop mechanism dynamics using closed-form kinematics solutions," *Multibody System Dynamics,* vol. 1, pp. 23-45, 1997.

[28] Y. Patel and P. George, "Parallel manipulators applications—a survey," *Modern Mechanical Engineering,* vol. 2, p. 57, 2012.

[29] J. M. Rico and B. Ravani, "Mobility of spatial multi-loop and mixed linkages," in *On advances in robot kinematics*, ed: Springer, 2004, pp. 133-142.

[30] S. Krut, M. Benoit, H. Ota, and F. Pierrot, "I4: A new parallel mechanism for Scara motions," in *2003 IEEE International Conference on Robotics and Automation (Cat. No.03CH37422)*, 2003, pp. 1875-1880 vol.2.

[31] R. Siegwart, P. Lamon, T. Estier, M. Lauria, and R. Piguet, "Innovative design for wheeled locomotion in rough terrain," *Robotics and Autonomous systems,* vol. 40, pp. 151-162, 2002.

[32] J. Schlaich and K. Schafer, "Design and detailing of structural concrete using strut-and-tie models," *Structural Engineer,* vol. 69, pp. 113-125, 1991.

[33] K. Liu, J. M. Fitzgerald, and F. L. Lewis, "Kinematic analysis of a Stewart platform manipulator," *IEEE Transactions on industrial electronics,* vol. 40, pp. 282-293, 1993.

[34] D. Basu and A. Ghosal, "Singularity analysis of platform-type multi-loop spatial mechanisms," *Mechanism and Machine Theory,* vol. 32, pp. 375-389, 1997.

[35] S. P. Lee, J. B. Badler, and N. I. Badler, "Eyes alive," in ACM Transactions on Graphics (TOG), 2002, pp. 637-644.

[36] R. P. Wildes, "Iris recognition: an emerging biometric technology," Proceedings of the IEEE, vol. 85, pp. 1348-1363, 1997.

[37] N. A. Dodgson, "Variation and extrema of human interpupillary distance," in Stereoscopic Displays and Virtual Reality Systems XI, 2004, pp. 36-47.

[38] P. Berg and M. Scherg, "Dipole models of eye movements and blinks," Electroencephalography and clinical Neurophysiology, vol. 79, pp. 36-44, 1991.